# Fluorescence Correlation Spectroscopy of Triplet States in Solution: A Theoretical and Experimental Study

**Jerker Widengren, Ülo Mets,† and Rudolf Rigler***

*Department of Medical Biophysics, MBB, Karolinska Institute, 171 77 Stockholm, Sweden*

*Received: March 17, 1995; In Final Form: June 26, 1995*[⊗]

A new approach for the study of singlet−triplet interactions of fluorophores in solution is presented, based on fluorescence correlation spectroscopy (FCS). The high excitation intensities used in FCS necessary for favorable S/N ratios can lead to significant intensity dependent distortions of the emission intensity distribution over the sample volume element from which fluorescence is collected and corresponding distortions of the fluorescence autocorrelation function. A theoretical outline of the photodynamical aspects of high excitation intensities in FCS is given. From this analysis, the rates of intersystem crossing and triplet decay as well as the excitation cross section of the fluorophore under investigation can be deduced. The triplet parameters of Rhodamine 6G (Rh6G) and Fluorescein isothiocyanate (FITC) have been determined in water and ethanol (Rh6G and FITC) and in methanol, propanol, and ethylene glycol (Rh6G). Also, the impact of potassium iodide and oxygen on the triplet parameters of Rh6G in water has been determined. The considerable spread in reference data and the relative simplicity of the method lead us to propose FCS as an appropriate method for the determination of triplet parameters of fluorophores in solution. Additionally, the comparatively high environmental sensitivity of these parameters indicates that triplet state monitoring by FCS can be used as a way of probing molecular microenvironments.

## Introduction

Attention has long been paid to the triplet state properties of laser dyes due to their influence on laser action. Moreover, the advent and extended use of fluorescence-based single molecule detection (SMD) in solution have again focused interest on the triplet properties of the fluorophores since molecules could be lost due to population of long-lived triplet states and an optimization of the number of photons emitted per molecule is required. The finite photochemical lifetime will set the ultimate limit. The triplet state properties play an important role considering that for many fluorophores, including Rh6G, irreversible photodegradation is thought to be proportional to the triplet state population.[1-4] The maximum fluorescence emission rate per molecule will be determined by the excitation intensity at which saturation of the excited singlet state is reached and by the extent of triplet state buildup. Mathies et al.[5] have derived optimal conditions for high-sensitivity fluorescence detection in the presence of both ground state depletion and photodestruction. However, to make full use of this approach, knowledge of the kinetic parameters for the triplet state is needed. Traditionally, most of the previous investigations of the triplet state kinetics of fluorophores in solution have been based on flash photolysis, applying pulsed excitation and subsequent measurement of $T-T_n$ absorption.[1,6-17] This requires a second probing beam and/or detection of phosphorescence generated in the triplet state decay. Alternatively, changes in absorption of triplet state quenchers,[18] singlet oxygen scavengers,[19,20] measurements of electron spin resonances,[14] lasing characteristics,[21-24] fluorescence saturation behavior,[25] and time-resolved photoacoustic calorimetry[26] have been used to deduce the amount of triplet buildup. Considering the importance of the triplet state properties, as mentioned above, it is surprising to find that data on the triplet states of fluorophores are not only scarce but also inconsistent between different reports. For Rh6G for instance, one of the most studied fluorophores, the reported values in air-saturated EtOH for intersystem crossing and triplet state lifetime respectively differ by more than an order of magnitude.[11-13,21,22,27,28]

In a first report[30] we have presented the principal analysis and an experimental realization of how to derive the kinetic parameters of the triplet state for a fluorophore (Rh6G) in solution by fluorescence correlation spectroscopy (FCS). The illumination of the sample volume element was assumed to be uniform. However, for a more generally valid analysis the nonuniform excitation of the sample volume element should be considered. In this paper, a more detailed analysis is given including the nonuniform illumination of the sample volume element. The validity has been tested at several different experimental conditions, and the results obtained have been compared to those reported in the literature as measured by other methods.

The conceptual basis and theory of FCS were laid more than 20 years ago.[31-33] FCS is based on the analysis of intensity fluctuations of fluorescent particles excited by a stationary light source. The particles under investigation are excited by a focused laser beam, which defines the sample volume element from which fluorescence is collected. In principle, information can be obtained about any dynamic process in the nanosecond time range and longer that manifests itself as a change in fluorescence intensity. Theoretical models and experimental realizations of FCS measurements of translational motion, uniform and laminar flow, chemical reactions,[34a,b] rotational motion,[33,35,36] and excited state lifetimes[33,36] have been reported. Until recently, long measurement times have been required in order to reach sufficient S/N ratios. Despite the potential

* Corresponding author.
† Currently on leave from the Institute of Chemical Physics and Biophysics, Tallinn, Estonia.
⊗ Abstract published in *Advance ACS Abstracts,* August 15, 1995.

0022-3654/95/2099-13368$09.00/0 

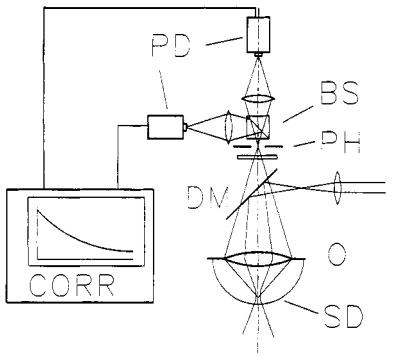


**Figure 1.** Schematic diagram of the experimental setup for FCS. SD = sample droplet, O = microscope objective, DM = dichroic mirror, PH = pinhole, BS = beam splitter, PD = photodiodes.

versatility of FCS, poor sensitivity and problems concerning the long time range photochemical and instrumental stability have restricted a wider use of FCS in the study of dynamics of molecules. However, by use of extremely small open volume elements in combination with confocal epi illumination, highly sensitive avalanche photodiodes for fluorescence detection, and well discriminative band-pass filters, it has been possible to improve S/N ratios in FCS measurements by several orders of magnitude.[37-40] The background level in our present FCS setup can be reduced so that it is approximately 3 orders of magnitude less than the fluorescence intensity of a single Rh6G molecule in aqueous solution. These improvements have removed the main obstacles preventing a more widespread application of FCS techniques and permit the detection of single molecules.[37,38] To obtain a small volume element and a sufficient S/B ratio, strong focusing of the excitation beam is often required. Very high excitation intensities can then be reached even with a moderate excitation power. This fact provides the basis for a convenient way in which singlet−triplet interactions can be monitored since a considerable population of the triplet state is generated. However, it also requires a somewhat modified theory for the expressions of the fluorescence autocorrelation functions, an outline of which is given below.

## Experimental Setup

The main experimental setup has been described before.[37-40] In brief, the light of an argon ion laser (Spectra Physics Model 165) operated at 514.5 nm (Rh6G) or 487 nm (FITC) was focused by a lens in front of an epi-illuminated microscope, reflected by a dichroic mirror (Leitz TK580), and refocused on the image plane of a water immersion objective (Zeiss Plan-Neofluar 63x NA 1.2). Laser power was regulated from the power supply of the laser and by inserting neutral OD filters (Schott) with varying attenuation. The power of the laser excitation under the objective was measured by a silicon photodiode (Photodyne 88XLC, silicon head Model No. 150). The fluorescent light was collected by the same objective and passed through a pinhole of 30 $\mu$m diameter in the image plane. The emitted light was then divided by a beam splitter and detected by two avalanche photodiodes (EG&G Model SPCM-100). Band-pass filters (Omega Optics 565DF50 or 535DF45) were placed in front of the detectors to discriminate against scattered laser light at the excitation wavelength and to minimize background from Raman scattered light of the water molecules in the sample volume element. The dimensions of the laser beam focus and the pinhole diameter in the confocal setup defined the sample volume from which fluorescent light was collected (Figure 1). The laser beam waist, $\omega_1$, was estimated from the measured dimensions of the beam at the focusing lens in front of the objective and by assuming a focusing of the laser beam in accordance with Gaussian optics. The laser beam waist obtained ($\omega_1 = 0.3$ $\mu$m $\pm$ 10%) was in good agreement with that deduced from FCS measurements. Fluorescence intensity fluctuations were recorded and analyzed in terms of a cross correlation function of the intensities registered by the two detectors separately. In this way the effect of the dead time of the detectors (250 ns) was avoided. The pulses of the photodiodes were passed to a PC-based correlator (ALV Model 5000), which calculated the cross correlation function over a logarithmic time scale. Data analysis was performed using the Marquardt nonlinear least squares algorithm.[41] The sample consisted of a hanging droplet of fluorophore solution placed under the microscope objective. Rh6G (Lambda Physik) and FITC (BBL Microbiology Systems) were prepared, without further purification, as stock solutions of 1 mM in EtOH and diluted with distilled water or 1 mM sodium carbonate buffer at pH 9, respectively. Alternatively the stock solution was diluted with ethylene glycol, methanol, 1-propanol (Merck p.a.) or ethanol (Kemetyl AB, spectroscopic purity). When measuring in the latter solvents, a cover-glass-corrected objective was used (Zeiss Plan-Neofluar 63x NA 1.2). To change the oxygen content of the fluorophore solutions in the hanging droplet (50 $\mu$L), the droplet was kept in an atmosphere of pure oxygen/argon gas of 1 atm for at least 15 min to equilibrate the solution. The measurements were done at room temperature and, if not otherwise stated, at air equilibrium. For determination of the decays of the excited singlet state, time-correlated single-photon counting was performed with a mode-locked cavity-dumped Rh6G dye laser emitting at 560 nm. Pulse frequency was 3.8 MHz. This instrumentation is described by Rigler et al.[42]

## Theoretical Background

Consider the case of a 3-D Gaussian excitation intensity distribution given by $\Phi(\bar{r},z) = \Phi_0 e^{-2\bar{r}^2/\omega_1} e^{-2z^2/\omega_2}$, where $z$ is the distance from the focal plane along the optical axis and $\bar{r}$ denotes the distance from the optical axis. $\omega_1$ and $\omega_2$ are the distances from the center of the volume element in the radial and axial direction, respectively, at which the detected fluorescence intensity has dropped by a factor of $e^2$. When translational diffusion of the fluorophores in and out of the sample volume element is the only noticeable dynamic process causing fluorescence fluctuations the normalized intensity autocorrelation function can be written as[35,40]

$$G_n(\tau) = \lim_{T\to\infty} \frac{1}{T}\int_0^T \frac{I(t+\tau)\, I(t)}{\langle I\rangle^2} dt = \frac{1}{N}\left(\frac{1}{1+4D\tau/\omega_1^2}\right)\left(\frac{1}{1+4D\tau/\omega_2^2}\right)^{1/2} + 1 \quad (1)$$

Here $N$ is the mean number of molecules within the sample volume element, $D$ is the translational diffusion coefficient of the fluorescent molecules, and $\langle I\rangle$ is the detected mean intensity. The detected fluorescence intensity profile will be determined by the laser beam profile and the projected dimensions of the pinhole. The total detected fluorescence intensity, $I(t)$, is given by[39,43]

$$I(t) = \int\int\int i(\bar{r},z,t)\, dV = \int\int\int q\mathrm{CEF}(\bar{r},z)\sigma_{exc}\Phi(\bar{r},z) \times c(\bar{r},z,t)\, dV \quad (2)$$

where $i(\bar{r},z,t)$ denotes the detected fluorescence per unit volume and $\sigma_{exc}$ is the excitation cross section of the fluorophore. The

parameter $q$ accounts for the quantum efficiency of the detectors, fluorescence quantum yield of the fluorophore, and attenuation of the fluorescence in the passage from the sample droplet to the detectors. $CEF(\bar{r},z)$ is the collection efficiency function, $c(\bar{r},z,t)$ denotes the concentration of fluorophores, and $\Phi(\bar{r},z)$ is the excitation intensity of the laser. In the derivation of eq 1 the distribution of $i(\bar{r},z,t)$ is assumed to be Gaussian in both the radial and axial directions. Equation 1 will also hold as an approximation for the case of a Lorentzian profile of $\Phi(\bar{r},z)$ along the optical axis.[39] In either of these cases $i(\bar{r},z,t)$ is assumed to be linear to $\Phi(\bar{r},z)$; that is, there is no saturation of the fluorophores. However, to optimize the fluorescence per molecule in the FCS measurements, high excitation intensities must be applied such that effects of increased triplet state population and saturation need to be considered. Also, eq 1 will not be fully valid if smaller pinholes are introduced so that $CEF(\bar{r},z)$ will not cover the extension of $\Phi(\bar{r},z)$. Additionally, distortions will be seen in the microsecond range of the experimental FCS curves due to transitions between singlet and triplet states of the fluorophores. Before treating these effects more in detail, the electronic states of the fluorophore involved in the process of fluorescence emission as well as the dimensions of the sample volume element must be defined.

**Electronic State Model.** The electronic states of Rh6G involved in the processes of fluorescence at 514.5 nm excitation wavelength can be modeled as shown in Figure 2. This model is similar to the one used to characterize fluorescence fluctuations of immobile pentacene molecules in $p$-terphenyl crystals[29,44-46] but will differ on a few points. $S_0$ denotes the ground singlet state, $S_1$ is the excited singlet state, and T is the lowest triplet state. $k_{12}$, $k_{21}$, $k_{23}$, and $k_{31}$ are the rate constants for excitation and deexcitation of the singlet state, intersystem crossing, and deexcitation of the triplet state, respectively. The rate of ground singlet state excitation, $k_{12}$, may be written as $\sigma_{exc}\Phi$, where $\sigma_{exc}$ is the excitation cross section of the ground singlet state and $\Phi$ is the excitation intensity. Since vibrational relaxation takes place in the picosecond time scale,[47] it can be neglected, as it will occur much faster than the other transitions. Also, the excitation cross section from the first excited singlet state to higher singlet states, $\sigma_{sn}$, can be neglected. At the above excitation wavelength $\sigma_{sn}$ will be as high as one-fourth of that from the ground singlet state.[9,48] However, since the relaxation from the higher singlet states (denoted by $k_{n1}$ in Figure 2) takes place in the subpicosecond time scale, excitation to higher singlet states is not considered in our model. Furthermore, the effects of stimulated emission, $\sigma_{21}$, or triplet−triplet absorption, $\sigma_{tn}$, need not be taken into consideration. Stimulated emission[9,49] and triplet−triplet absorption[11] will be negligibly small when exciting with a wavelength out of the emission band and when the concentration of the fluorophores is in the nanomolar range. The excitation and emission dipole moments of the fluorophore molecules can be treated as isotropic since the rotation of the molecules will take place in the subnanosecond time scale. Due to the fact that the triplet state lifetime ($1/k_{31}$) is quite long compared to that of the singlet state ($1/k_{21}$) and that the phosphorescence quantum yield from the triplet state is quite low, the triplet state can be considered as a nonluminescent state.[14] Finally, the simplifying assumption is made that the fluorophore is photochemically intact. Since the photochemical lifetime far exceeds the time frame for the singlet−triplet transitions,[50] photobleaching is not included in the model used to describe the singlet−triplet interactions.

**The Sample Volume Element.** The intensity of the focused laser beam was considered to be Gaussian in the radial direction and Lorentzian in the axial direction:

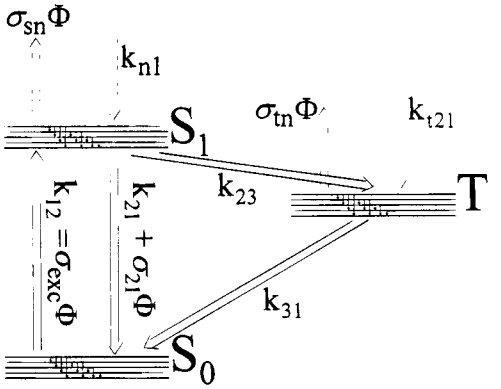


**Figure 2.** Electron state model of Rh6G and its rate constants. See text for further description.

$$\Phi(\bar{r},z) = \frac{2P}{\pi\omega^2(z)} e^{-2(|\bar{r}|^2/\omega^2(z))} \tag{3}$$

where $P$ is the power of the laser and $\bar{r}$ denotes the coordinate of the emitter in the radial plane. The radius of the focused laser beam, $\omega(z)$, is given by

$$\omega^2(z) = \omega_1^2 + z^2 \tan^2 \delta \tag{4}$$

where $\delta$ is the focusing angle of the laser beam in the sample at $1/e^2$ intensity and $z$ is the distance from the focal plane along the optical axis. The detected time-averaged fluorescence intensity at a point $(\bar{r},z)$, denoted by $\bar{i}(\bar{r},z)$, whose spatial distribution defines the sample volume element can then be written as

$$\bar{i}(\bar{r},z) = k_{21} q CEF(\bar{r},z)\, \bar{S}_1(\bar{r},z)\, \bar{c}(\bar{r},z) \tag{5}$$

$\bar{S}_1(\bar{r},z)$ denotes the fraction of the fluorophores being in the excited singlet state (see eq 9), and $\bar{c}(\bar{r},z)$ is the steady state fluorophore concentration. $CEF(\bar{r},z)$ is the collection efficiency function, which is determined by the numerical aperture, magnification, and resolution limit of the microscope objective as well as by the diameter of the pinhole as

$$CEF(\bar{r},z) = \frac{1}{\Delta}\int T(\bar{r}_p)\, PSF(\bar{r}_p,\bar{r},z)\, d\bar{r}_p \tag{6}$$

The integration is made over the focal plane. $\Delta$ is a normalization factor given the value $\int T(\bar{r}_p)\, PSF(\bar{r}_p,0,0)\, d\bar{r}_p$. $T(\bar{r}_p)$ denotes the transmission function of the projected pinhole at a point $\bar{r}_p$ on the focal plane and is given by

$$T(\bar{r}_p) = \mathrm{circ}(\bar{r}_p/s_0) \equiv \begin{cases} 1 \text{ if } |\bar{r}_p| \le s_0 \\ 0 \text{ if } |\bar{r}_p| > s_0 \end{cases} \tag{7}$$

Here $s_0$ represents the projection of the pinhole radius on the focal plane. The point spread function, $PSF(\bar{r}_p,\bar{r},z)$, describes the intensity distribution in the focal plane from a point source located at $(\bar{r},z)$. It can be written as

$$PSF(\bar{r}_p,\bar{r},z) = \frac{\mathrm{circ}((\bar{r}_p - \bar{r})/R(z))}{\pi R^2(z)} \tag{8}$$

where $R^2(z) = R_0^2 + z^2 \tan^2 \alpha$, with $R_0$ denoting the resolution limit of the objective and $\alpha$ being the aperture half-angle of the microscope objective.

**The Modified Correlation Function.** Applying the electron state model described above to the case in FCS, where diffusing fluorophore molecules are exposed to a laser beam under the microscope objective, the arising fluorescence fluctuations will be caused either by diffusion in and out of the sample volume element or by the fluorescent molecules entering and leaving the triplet state. The fluorescence intensity fluctuations from translational diffusion and from singlet−triplet transitions can be considered independent of each other. Assuming that the singlet−triplet transitions take place on a time scale much faster than the diffusion time, $\tau_D \approx \omega_1^2/4D$, the fluctuations can be treated separately in a fast time range ($\approx\mu$s), where the fluorophores can be considered as immobile and where singlet−triplet interactions take place and in a slow time range ($\approx$100 $\mu$s), where the singlet−triplet interactions will be in a steady state, while the fluorophores are moving.

**Fast Time Range.** The population of the electronic states of the fluorophore, according to the electron state model, consists of the populations in the ground singlet, $S_0$, the excited singlet, $S_1$, and the lowest triplet, T, states. The fluorophore concentration can be written as

$$c(\bar{r},z,t) = c(\bar{r},z,t)[S_1(\bar{r},z,t) + S_0(\bar{r},z,t) + T(\bar{r},z,t)] \quad (9)$$

so that

$$[S_1(\bar{r},z,t) + S_0(\bar{r},z,t) + T(\bar{r},z,t)] = 1$$

The probability of occupying one of the three different states at a point $(\bar{r},z)$ can be expressed in terms of the rate constants by solving the following system of three first-order differential equations:

$$\frac{d}{dt}\begin{pmatrix} S_0(\bar{r},z,t) \\ S_1(\bar{r},z,t) \\ T(\bar{r},z,t) \end{pmatrix} = \begin{bmatrix} -k_{12}(\bar{r},z) & k_{21} & k_{31} \\ k_{12}(\bar{r},z) & -(k_{23}+k_{21}) & 0 \\ 0 & k_{23} & -k_{31} \end{bmatrix} \begin{pmatrix} S_0(\bar{r},z,t) \\ S_1(\bar{r},z,t) \\ T(\bar{r},z,t) \end{pmatrix} \quad (10)$$

where $k_{12}(\bar{r},z) = \sigma_{exc}\Phi(\bar{r},z)$. One can assume that the decay of the singlet state by fluorescence or internal conversion is much faster than either of the processes of intersystem crossing or triplet state decay, i.e.:

$$k_{21} \gg k_{23}, k_{31} \quad (11)$$

In the process of fluorescence, a photon is released and the fluorophore molecule enters its ground singlet state. Defining the time of fluorescence emission as $t = 0$, one can write

$$\begin{pmatrix} S_0(\bar{r},z,0) \\ S_1(\bar{r},z,0) \\ T(\bar{r},z,0) \end{pmatrix} = \begin{pmatrix} 1 \\ 0 \\ 0 \end{pmatrix} \quad (12)$$

Applying the assumption of eq 11 and the boundary condition of eq 12 to the above system of differential equations and assuming a stationary excitation intensity, one obtains the probabilities of occupying the different electronic states as a function of time, $t$, after photon release:

$$S_0(\bar{r},z,t) = \frac{k_{21}k_{31}}{k_{12}(\bar{r},z)(k_{23}+k_{31}) + k_{21}k_{31}} e^{\lambda_1(\bar{r},z)t} + \frac{k_{12}(\bar{r},z)}{k_{12}(\bar{r},z) + k_{21}} e^{\lambda_2(\bar{r},z)t} + \frac{k_{12}(\bar{r},z)k_{21}k_{23}}{(k_{12}(\bar{r},z) + k_{21})[k_{12}(\bar{r},z)(k_{23}+k_{31}) + k_{21}k_{31}]} e^{\lambda_3(\bar{r},z)t} \quad (13a)$$

$$S_1(\bar{r},z,t) = \frac{k_{12}(\bar{r},z)k_{31}}{k_{12}(\bar{r},z)(k_{23}+k_{31}) + k_{21}k_{31}} e^{\lambda_1(\bar{r},z)t} - \frac{k_{12}(\bar{r},z)}{k_{12}(\bar{r},z) + k_{21}} e^{\lambda_2(\bar{r},z)t} + \frac{k_{12}^2(\bar{r},z)k_{23}}{(k_{12}(\bar{r},z) + k_{21})[k_{12}(\bar{r},z)(k_{23}+k_{31}) + k_{21}k_{31}]} e^{\lambda_3(\bar{r},z)t} \quad (13b)$$

$$T(\bar{r},z,t) = \frac{k_{12}(\bar{r},z)k_{23}}{k_{12}(\bar{r},z)(k_{23}+k_{31}) + k_{21}k_{31}} e^{\lambda_1(\bar{r},z)t} - \frac{k_{12}(\bar{r},z)k_{23}}{k_{12}(\bar{r},z)(k_{23}+k_{31}) + k_{21}k_{31}} e^{\lambda_3(\bar{r},z)t} \quad (13c)$$

where the eigenvalues are given by

$$\lambda_1(\bar{r},z) = 0 \quad (14a)$$

$$\lambda_2(\bar{r},z) = -(k_{21} + k_{12}(\bar{r},z)) \quad (14b)$$

$$\lambda_3(\bar{r},z) = -\left[k_{31} + \frac{k_{12}(\bar{r},z)k_{23}}{k_{12}(\bar{r},z) + k_{21}}\right] \quad (14c)$$

The first eigenvalue, $\lambda_1$, will be 0, indicating that the populations in the three states will approach a steady state as $t \rightarrow \infty$. This follows from the fact that the triplet model constitutes a closed system assuming a constant total population and no photobleaching. The second eigenvalue, $\lambda_2$, will be of high magnitude and represents the so-called "antibunching" term.[33,51,52] It will not be dealt with further in this study since its magnitude is too high to be measured properly with the time resolution of our present instrumentation. The magnitude of the third eigenvalue, $\lambda_3$, is roughly related to the rate at which the buildup of the triplet state population takes place. Its inverse will be referred to as the bunching time, $\tau_T$. The probability, $P_D$, for the detection of a photon emitted at time $t + \tau$ in position $(\bar{r}_2,z_2)$ from a particle that had absorbed and emitted a photon in $(\bar{r}_1,z_1)$ at time $t$ will be

$$P_D(\bar{r}_2,z_2,\bar{r}_1,z_1,\tau) = P(\bar{r}_2,z_2,\bar{r}_1,z_1,\tau)\, P_1(\bar{r}_2,z_2,\tau) \quad (15)$$

where

$$P(\bar{r}_2,z_2,\bar{r}_1,z_1,\tau) = \delta[(\bar{r}_2,z_2) - (\bar{r}_1,z_1)] \quad (16)$$

and

$$P_1(\bar{r}_2,z_2,\tau) = k_{21}q\mathrm{CEF}(\bar{r}_2,z_2)\, S_1(\bar{r}_2,z_2,\tau) \quad (17)$$

Exchange between $S_1$ and $S_0$ (given from $\lambda_2(\bar{r},z)$) takes place in the nanosecond time range. In the microsecond time range, the $e^{\lambda_2(\bar{r},z)}$ term in eq 13b will vanish. Including eqs 13b and 13c in eq 17 gives

$$P_1(\bar{r}_2,z_2,\tau) = k_{21}q\mathrm{CEF}(\bar{r}_2,z_2) \times \bar{S}_1(\bar{r}_2,z_2)\left[\left[\frac{\bar{T}(\bar{r}_2,z_2)}{1-\bar{T}(\bar{r}_2,z_2)}\right]e^{\lambda_3(\bar{r}_2,z_2)\tau} + 1\right] \quad (18)$$

Here, bars over $S_1$ and $T$ denote steady state populations, which are given by the first terms in eq 13b and eq 13c, respectively. In practice, the event of a fluorescence photon emission at a point $(\bar{r},z)$ is governed by two stochastic variables, which are independent and whose fluctuations occur on different time scales. The first of these is the population of the excited singlet state $S_1(\bar{r},z,t)$, and the second is the concentration of fluorophores, $c(\bar{r},z,t)$, which is governed by Poissonian statistics so that

$$\langle[\delta c(\bar{r},z,t)]^2\rangle = \bar{c}(\bar{r},z) \tag{19}$$

The fluorescence intensity fluctuations detected from the sample volume element will then be

$$\delta i(t) = \int k_{21} q\mathrm{CEF}(\bar{r},z)\, \delta[c(\bar{r},z,t)\, S_1(\bar{r},z,t)]\, \mathrm{d}V \tag{20}$$

Regarding $i(\bar{r},z,t)$ as a doubly stochastic Poissonian process,[53] the variance of $i(\bar{r},z,t)$ can be written

$$\begin{aligned}\mathrm{Var}[i(\bar{r},z,t)] = \langle[\delta i(\bar{r},z,t)]^2\rangle = \\ [k_{21} q\mathrm{CEF}(\bar{r},z)\, \bar{S}_1(\bar{r},z)]^2 \bar{c}(\bar{r},z) + \\ [k_{21} q\mathrm{CEF}(\bar{r},z)\, \bar{S}_1(\bar{r},z)]\bar{c}(\bar{r},z)[P_1(\bar{r},z,0) - \\ k_{21} q\mathrm{CEF}(\bar{r},z)\, \bar{S}_1(\bar{r},z)] = \\ [k_{21} q\mathrm{CEF}(\bar{r},z)\, \bar{S}_1(\bar{r},z)]\bar{\imath}(\bar{r},z)\left[1 + \frac{\bar{T}(\bar{r},z)}{1-\bar{T}(\bar{r},z)}\right]\end{aligned} \tag{21}$$

where the first term is the variance due to the fluctuations of $c(\bar{r},z,t)$ alone and the second term is the "excess" variance originating from the additional fluctuations of $i(\bar{r},z,t)$ due to singlet−triplet transitions. Denoting these fluctuations by $\delta i_s(t)$ and $\delta i_f(t)$, respectively, the corresponding correlation function of the fluorescence intensity in the fast time range integrated over the whole sample volume element will be

$$\begin{aligned}G_f(\tau) = \langle[\langle i\rangle + \delta i(t)][\langle i\rangle + \delta i(t+\tau)]\rangle = \langle i\rangle^2 + \\ \langle \delta i_f(t)\, \delta i_f(t+\tau)\rangle + \langle \delta i_s(t)\, \delta i_s(t+\tau)\rangle = \langle i\rangle^2 + \\ \int\int i(\bar{r}_1,z_1)\, P_D(\bar{r}_1,z_1,\bar{r}_2,z_2,\tau)\, \mathrm{d}V_1\, \mathrm{d}V_2 = \langle i\rangle^2 + \\ \int i(\bar{r}_2,z_2)\, P_1(\bar{r}_2,z_2,\tau)\, \mathrm{d}V_2\end{aligned} \tag{22}$$

where brackets signify time average and $\langle i\rangle = \int \bar{\imath}(\bar{r},z)\, \mathrm{d}V$. It can be noted that the first term in eq 21, arising from fluctuations of $c(\bar{r},z,t)$ alone, will remain constant in the fast time range. By the use of eqs 5 and 18, $G_f(\tau)$ can be written as

$$\begin{aligned}G_f(\tau) = \int \frac{\bar{\imath}^2(\bar{r}_2,z_2)}{\bar{c}(\bar{r}_2,z_2)} \frac{\bar{T}(\bar{r}_2,z_2)}{1-\bar{T}(\bar{r}_2,z_2)} \mathrm{e}^{\lambda_3(\bar{r}_2,z_2)\tau}\, \mathrm{d}V_2 + \\ \int k_{21} q\mathrm{CEF}(\bar{r}_2,z_2)\, \bar{S}_1(\bar{r}_2,z_2)\, \bar{\imath}(\bar{r}_2,z_2)\, \mathrm{d}V + \langle i\rangle^2\end{aligned} \tag{23}$$

**Slow Time Range.** At long time scales, eq 16 will become[54]

$$P(\bar{r}_1,z_1,\bar{r}_2,z_2,\tau) = \frac{1}{(4\pi D\tau)^{3/2}} \mathrm{e}^{-[(\bar{r}_2,z_2)-(\bar{r}_1,z_1)]^2/4D\tau} \tag{24}$$

Since the population of the electronic states can be considered to be in their steady states, eq 18 will be

$$P_1(\bar{r}_2,z_2,\tau) = k_{21} q\mathrm{CEF}(\bar{r}_2,z_2)\, \bar{S}_1(\bar{r}_2,z_2) \tag{25}$$

The autocorrelation in the slow time range can be written as

$$G_s(\tau) = \langle[\langle i\rangle + \delta i_s(t)][\langle i\rangle + \delta i_s(t+\tau)]\rangle = \langle i\rangle^2 + \langle \delta i_s(t)\, \delta i_s(t+\tau)\rangle$$

where $\delta i_s(\tau)$ denotes the intensity fluctuations in the slow time range and is given by

$$\delta i_s(t) = \int k_{21} q\mathrm{CEF}(\bar{r},z)\, \bar{S}_1(\bar{r},z)\, \delta c(\bar{r},z,t)\, \mathrm{d}V \tag{26}$$

After insertion of eqs 5, 24, and 25 the correlation function will take the form

$$G_s(\tau) = \langle i\rangle^2 + \int\int \frac{\bar{\imath}(\bar{r}_2,z_2)\, \bar{\imath}(\bar{r}_1,z_1)}{(\bar{c}(r_2,z_2))^{1/2}(\bar{c}(r_1,z_1))^{1/2}} \times \frac{1}{(4\pi D\tau)^{3/2}} \mathrm{e}^{-[(\bar{r}_2,z_2)-(\bar{r}_1,z_1)]^2/4D\tau}\, \mathrm{d}V_1\, \mathrm{d}V_2 \tag{27}$$

If $\bar{\imath}(\bar{r},z)$ would have a Gaussian shape in the radial as well as in the axial dimension and with the assumption of a constant $\bar{c}(\bar{r},z)$ over space (no photobleaching), normalization of eq 27 by $\langle i\rangle^2$ yields eq 1. However, in the case that $\bar{\imath}(\bar{r},z)$ has a non-Gaussian profile, due to saturation and noticeable triplet state populations of the fluorophores combined with the influence of a narrow CEF$(\bar{r},z)$, eq 27 will be different.

## Evaluation of the Autocorrelation Functions

**Fast Time Range.** It can be seen from eq 23 that in the experimental autocorrelation (AC) function the intensity dependent parameters $\bar{T}$ and $\lambda_3$ appear as weighted integrals over the sample volume element. Therefore, instead of a single-exponential decay, a continuous distribution of exponentials over some interval of $\lambda_3$ can be expected. However, due to moderate S/N ratios in this fast time range and a narrow CEF$(\bar{r},z)$, which will restrict the span of $\Phi(\bar{r},z)$ over the sample volume element, this distribution is usually not resolved. To improve the accuracy of the returned parameters and to illustrate the specific features of signal averaging in FCS, we analyzed this distribution. Following eq 23, $\bar{T}$ could be spatially averaged as

$$\bar{T}_{eq} = \frac{\int \bar{T}(\bar{r},z) \dfrac{\bar{\imath}^2(\bar{r},z)}{1-\bar{T}(\bar{r},z)}\, \mathrm{d}V}{\int \dfrac{\bar{\imath}^2(\bar{r},z)}{1-\bar{T}(\bar{r},z)}\, \mathrm{d}V} \tag{28}$$

The average bunching time can be defined from the time integral:

$$\bar{\tau}_T = -\frac{1}{\lambda_3} \equiv \int_0^\infty b(\tau)\, \mathrm{d}\tau$$

where

$$b(\tau) = \frac{G_f(\tau) - G_f(\infty)}{G_f(0) - G_f(\infty)} = \frac{\int \dfrac{\bar{\imath}^2(\bar{r},z)}{\bar{c}(\bar{r},z)} a(\bar{r},z) \mathrm{e}^{\lambda_3(\bar{r},z)\tau}\, \mathrm{d}V}{\int \dfrac{\bar{\imath}^2(\bar{r},z)}{\bar{c}(\bar{r},z)} a(\bar{r},z)\, \mathrm{d}V}$$

so that

$$\bar{\tau}_T = \int_0^\infty b(\tau)\,d\tau = \frac{\int \frac{\bar{i}^2(\bar{r},z)}{\bar{c}(\bar{r},z)} a(\bar{r},z) 1/\lambda_3(\bar{r},z)\,dV}{\int \frac{\bar{i}^2(\bar{r},z)}{\bar{c}(\bar{r},z)} a(\bar{r},z)\,dV} \quad (29)$$

Here, eq 23 has been used, and $a(\bar{r},z) = \bar{T}(\bar{r},z)/1 - \bar{T}(\bar{r},z)$. Due to relatively narrow distributions of $\lambda_3$, we expect the result of the least squares fitting of the experimental AC functions to a single exponential to be sufficiently well approximated by these averages:

$$G_f(\tau) = \left[\frac{1}{N}\left[\frac{\bar{T}_{eq}}{1-\bar{T}_{eq}} e^{\bar{\lambda}_3\tau} + 1\right] + 1\right]\langle i\rangle^2 = \left[\frac{1}{N(1-\bar{T}_{eq})}[\bar{T}_{eq} e^{\bar{\lambda}_3\tau} + 1 - \bar{T}_{eq}] + 1\right]\langle i\rangle^2 \quad (30)$$

Here, $N$ denotes the mean number of fluorophore molecules within the sample volume element (However, in the fast time range the actual mean number of fluorescent molecules will be $N(1 - \bar{T}_{eq})$, since the population of the triplet can in practice be considered as nonluminescent.) In the case of a high ratio of $k_{23}/k_{31}$ and at medium low intensities, the relative span of $e^{\lambda_3(\bar{r},z)}$ within the sample volume element will increase. Then an approximation of $\int e^{\lambda_3(\bar{r},z)\tau}\,dV$ as a single exponential could be misleading. Following eq 29, $\tau_T$ was under those conditions instead estimated from the experimental curve as

$$\bar{\tau}_T = \int_0^{\tau'} \frac{\int G_{exp}(\tau) - G_s(\tau')\,dV}{\int G_{exp}(0) - G_s(\tau')\,dV}\,d\tau \quad (31)$$

where $G_{exp}(\tau)$ is the experimental FCS curve, $G_s(\tau)$ denotes the fitted correlation function in the slow time range, and $\tau'$ signifies a correlation time chosen so that it is far longer than the time range of the singlet−triplet interactions. In other words, instead of using a least squares fitting procedure, $\bar{\tau}_T$ was obtained from the time integral of the singlet−triplet fluctuation term of the autocorrelation function in the fast time range (first term in eq 23). In general, the precision of using eq 31 in the determination of $\bar{\tau}_T$ was not as good as the use of eq 30. In practice, it was also found that the experimental determination of $\bar{\tau}_T$ from a single exponential gave almost identical results compared to using eq 31 but with improved precision and stability. The use of eq 31 was therefore restricted to the above mentioned cases where the collection of $e^{\lambda_3(\bar{r},z)}$ could be expected not to be well approximated by a single exponential.

**Slow Time Range.** Elson and Madge[31] have compared the shapes of 2-D AC functions for a rectangular profile of $\bar{i}(\bar{r})$ to a Gaussian-shaped one and found the difference to be relatively small. In general, with a small pinhole and hence a narrow CEF$(\bar{r},z)$, a change in the distribution of $\bar{S}_1(\bar{r},z)$ will lead to comparatively minor distortions of the shape of the experimental AC function in the slow time range. Considering also that there are a number of diverse effects influencing $\bar{i}(\bar{r},z)$, it is very difficult to present a quantitative analysis that could be tested experimentally (see below). The correlation function describing the fluorescence fluctuations in the slow time range as given by eq 27 cannot, under our experimental conditions, be expressed in a straightforward analytical form, but rather needs to be calculated numerically. The main topic of this work is to characterize the singlet−triplet fluctuations. Our approach here will therefore be limited to use, when necessary, a slightly modified equation for the slow time range compared to that of eq 1 in the fitting procedure. In practice, the expression of eq 1 was applicable to AC functions measured at low intensities, whereas the fitting of the AC functions measured at high intensities did not give satisfactory results. In these cases, the introduction in eq 1 of a correction term in the form of a second diffusional correlation term produced improved fittings:

$$G(\tau) = \left[\frac{1}{N}\left[R\left(\frac{1}{1+\tau/\tau_1}\right)\left(\frac{1}{1+\tau/K\tau_1}\right)^{1/2} + (1-R)\left(\frac{1}{1+\tau/\tau_2}\right)\left(\frac{1}{1+\tau/K\tau_2}\right)^{1/2}\right] + DC\right]\langle i\rangle^2 \quad (32)$$

where $\tau_1$ and $\tau_2$ denote the two diffusional correlation times, $0 < R < 1$, $K = [\omega_2/\omega_1]^2$, and DC denotes $g(\tau)$ as $\tau \to \infty$. This expression corresponds to a volume element profile described by a sum of two Gaussian distributions. One possible reason for the second Gaussian term is the enhanced contribution of the "wings" of the CEF$(\bar{r},z)$ in the case of fluorescence saturation (see Figure 4a,b and Rigler et al.[39]).

**The Full Correlation Function.** Combining the expressions of eqs 30 and 32 and considering fluorescence fluctuations from translational diffusion, $\delta i_s(t)$, as independent from those due to singlet−triplet transitions, $\delta i_f(t)$, the normalized correlation function will take the form

$$G_n(\tau) = \frac{\langle[(\langle i\rangle + \delta i_s(t) + \delta i_f(t))(\langle i\rangle + \delta i_s(t+\tau) + \delta i_f(t+\tau))]\rangle}{\langle i\rangle^2} = \frac{\langle \delta i_s(t)\,\delta i_s(t+\tau)\rangle + \langle \delta i_f(t)\,\delta i_f(t+\tau)\rangle + \langle i\rangle^2}{\langle i\rangle^2} = \frac{1}{N}\left[R\left(\frac{1}{1+\tau/\tau_1}\right)\left(\frac{1}{1+\tau/K\tau_1}\right)^{1/2} + (1-R)\left(\frac{1}{1+\tau/\tau_2}\right)\left(\frac{1}{1+\tau/K\tau_2}\right)^{1/2} + \frac{\bar{T}_{eq}}{1-\bar{T}_{eq}} e^{\bar{\lambda}_3\tau}\right] + DC$$

which since $\tau_1, \tau_2 \gg 1/\bar{\lambda}_3$, may be written as

$$G(\tau) = \frac{1}{N(1-\bar{T}_{eq})}\left[R\left(\frac{1}{1+\tau/\tau_1}\right)\left(\frac{1}{1+\tau/K\tau_1}\right)^{1/2} + (1-R)\left(\frac{1}{1+\tau/\tau_2}\right)\left(\frac{1}{1+\tau/K\tau_2}\right)^{1/2}\right][\bar{T}_{eq} e^{\bar{\lambda}_3\tau} + 1 - \bar{T}_{eq}] + DC \quad (33)$$

**The Amplitude of the Experimental Intensity Autocorrelation Function.** The amplitude of the autocorrelation function (eq 33) reflects the fluctuation of the number of fluorophores being in either $S_0$ or $S_1$. One might expect the amplitude of $G(\tau)$ to increase monotonically with rising intensities since $\bar{T}_{eq}$ will increase. However, this is not what is observed (Figure 3a). There are several phenomena influencing the amplitude of the experimental AC functions. The background intensity, which mainly consists of Raman scattering from water molecules, will be linear with respect to the excitation intensity (Figure 3b), while the fluorescence intensity will level out at higher excitation intensities (Figure 3c). Since the amplitude of the correlation function will be influenced by the background with a factor $[1 - I_b/(I_s + I_b)]$,[32] where $I_b$ and $I_s$ are the detected background and signal intensity respectively, a decreased amplitude will result as soon as saturation of the fluorophores is present. At low enough intensities, where $I_s$ is approaching the dark-count level of the photodetectors, the amplitude will be reduced for the same reason. From eqs 3 and 13b it follows that when continuously raising the laser beam power, the saturation of the fluorophores will first appear in

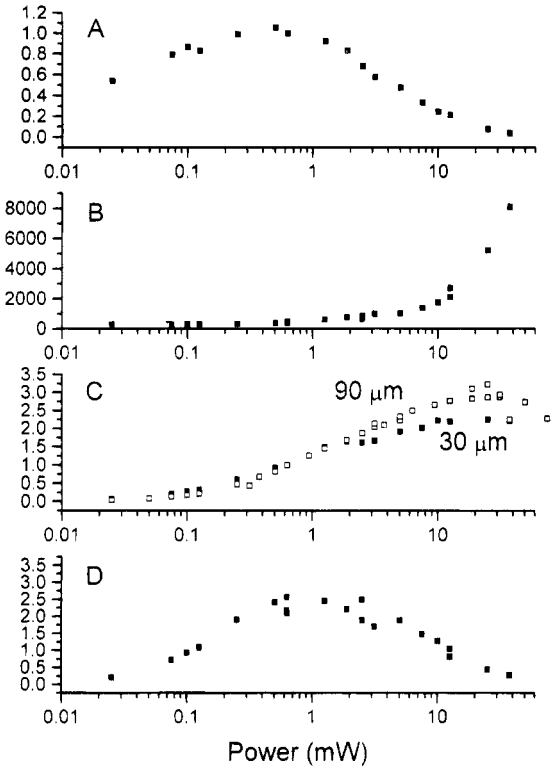


**Figure 3.** Fluorescence characteristics of Rh6G (3 nM) as a function of excitation power. Plotted are the amplitude ($1/N'$) of the correlation function (A), background counts (B), background-corrected fluorescence intensity (C), and S/B ratio (D). Data were collected with the experimental setup as described above (pinhole diameter 30 $\mu$m). In (C) a measurement series with a 90 $\mu$m pinhole has been added. (A), (C), and (D) are given in arbitrary units.

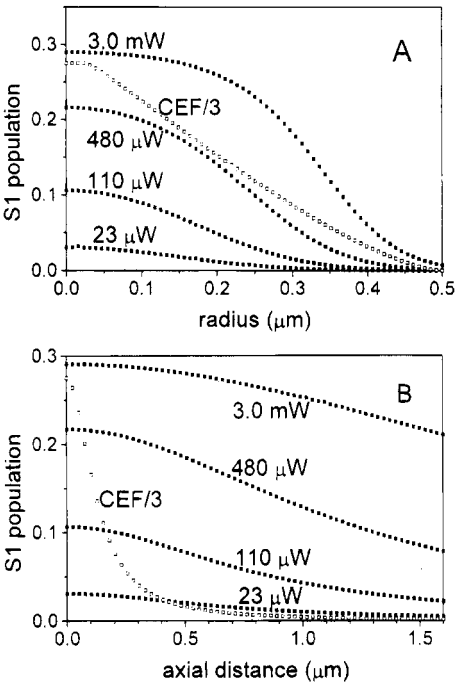


**Figure 4.** Simulation of $S_{1eq}(\bar{r},z)$ for Rh6G under different excitation intensities in the radial (A) and axial (B) dimensions, respectively. Also shown are the calculated CEF profiles (30 $\mu$m pinhole). The sample volume element is defined from the distances in the two directions, respectively, at which the detected fluorescence mean intensity, $\bar{i}(\bar{r},z)$, has dropped by a factor of $e^2$ compared to the intensity in the center of the focal plane, $\bar{i}(0,0)$. A smaller pinhole diameter will produce a sample volume element which is changed less at higher intensities, since CEF-$(\bar{r},z)$ is not influenced and will be the limiting factor of $\bar{i}(\bar{r},z)$. However, the detected fluorescence per molecule per second will also be less (Figure 3c).

the center of the beam in the focal plane. This will lead to a broadening of the fluorescence intensity profile (proportional to $\bar{S}_1(\bar{r},z)$, given by the first term in eq 13b), thereby increasing the sample volume element and decreasing the amplitude of $G(\tau)$ (Figure 4). Consequently, with the setting used here, the sample volume element will be determined mainly by the CEF-$(\bar{r},z)$ at high intensities (Figure 4). Additional distortion of the sample volume element can result from photobleaching. Even though only a small fraction of the fluorophores are bleached in one passage through the laser beam, the application of continuous laser excitation will lead to a gradually reduced concentration in the beam center. The presence of a depletion of this kind is another reason that is likely to necessitate a modification of the original AC function due to translational diffusion as given by eq 1. For Rh6G in water, the exchange rate of fluorophore molecules by translational diffusion in and out of the sample volume element will in our case, with a beam radius of $\approx$0.3 $\mu$m, dominate over the rate of photodecomposition ($k_d = \Phi_d \bar{S}_1$, where $\Phi_d = 1.8 \times 10^{-5}$ is the quantum efficiency of photobleaching[50]). Numerical simulations using a Crank–Nicholson procedure similar to the one used by Peters et al.[55] show that at high intensities the concentration depletion in the beam center will then make up a few percent (Figure 5). Due to the diversity of processes influencing the amplitudes of the experimental FCS curves, the amplitude of the correlation function of eq 33 was simplified to $1/N'$, where $N'$ simply is the inversed amplitude of the correlation function given by $N(1 - \bar{T}_{eq})$ and is influenced by the processes mentioned above. $R$ and $(1 - R)$ are the relative fractions of the two diffusion times applied, following eqs 32 and 33.

$$G(\tau) = \frac{1}{N'}\left[R\left(\frac{1}{1+\tau/\tau_1}\right)\left(\frac{1}{1+\tau/K\tau_1}\right)^{1/2} + (1-R)\left(\frac{1}{1+\tau/\tau_2}\right)\left(\frac{1}{1+\tau/K\tau_2}\right)^{1/2}\right][(1-\bar{T}_{eq}) + \bar{T}_{eq}e^{\bar{\tau}/\bar{\tau}_T}] + DC \quad (34)$$

The above equation was used in the fitting procedure, where the parameters $N'$, $R$, $\tau_1$, $\tau_2$, $K$, $\bar{T}_{eq}$, $\tau_T$ and DC were allowed to vary freely.

## Results and Discussion

For determining the rate constants $k_{23}$ and $k_{31}$, as well as the excitation cross section $\sigma_{exc}$, fluorescence autocorrelation (AC) functions at different excitation intensities were measured. These data were numerically fitted to eq 34. In this way, one obtains two equations, eqs 28 and 29, for each one of the AC functions relating the experimentally determined values of $\bar{T}_{eq}$ and $\bar{\tau}_T$ to the three unknown parameters $k_{23}$, $k_{31}$, and $\sigma_{exc}$. By plotting these experimental values of $\bar{T}_{eq}$ and $\bar{\tau}_T$ as a function of excitation intensity and by making a simultaneous nonlinear least squares fit to the expressions of eqs 28 and 29, respectively, the three unknown parameters could be determined. This corresponds to solving an overdetermined equation system of independent expressions of $k_{23}$, $k_{31}$, and $\sigma_{exc}$. In this way, a more accurate determination of the parameters could be obtained. The integrals of eqs 28 and 29 were calculatednumerically by Romberg's method, and the total decay rate of the excited singlet state ($k_{21} + k_{23}$) was fixed at the value 247 $\times 10^6$ s$^{-1}$ obtained from time-correlated single-photon-counting

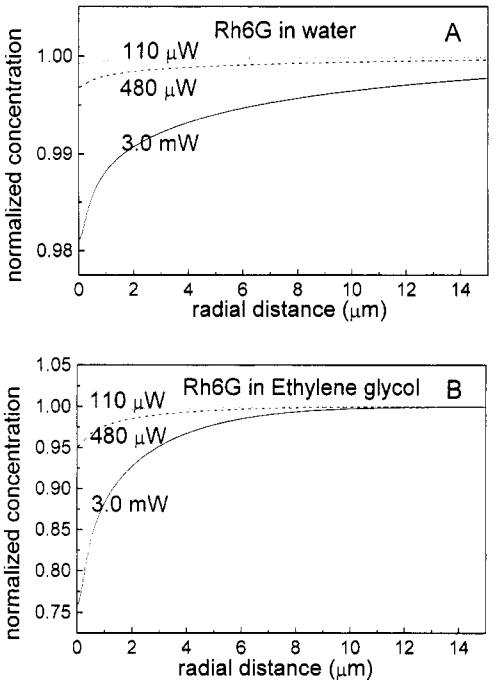


**Figure 5.** Simulations of how the concentration of Rh6G molecules is changed in the sample volume element at constant irradiation having water (A) and ethylene glycol (B) as solvents, respectively. The concentration is governed by the diffusion equation with a negative source term arising from photodegradation: $\nabla^2 c(\bar{r},z,t) = -D(\partial c(\bar{r},z,t)/\partial t) - k_d \bar{T}(\bar{r},z)\ c(\bar{r},z,t)$. The photodegradation is assumed to be proportional to the triplet state population, and $k_d$ is set equal to $(k_{31}/k_{23})\Phi_d k_{21}$, where $\Phi_d$ is the photodestruction yield per excitation cycle. $\Phi_d$ was set to $1.8 \times 10^{-5}$, obtained from Soper et al.,[50] and $D$ was $2.8 \times 10^{-6}$ cm$^2$/s (water) and $0.14 \times 10^{-6}$ cm$^2$/s (ethylene glycol), respectively. A numerical simulation using a two-dimensional Crank–Nicholson approach was used. The ≈20 times faster diffusion of Rh6G in water will reduce the concentration depletion in the beam center to, at most, a few percent. In ethylene glycol, however, assuming $\Phi_d$ to be the same as in water, the slow diffusion through the sample volume element will cause the depletion to be much more pronounced.

measurements for Rh6G and at $260 \times 10^6$ s$^{-1}$ for FITC.[56] The concentrations of the fluorophores were on the order $10^{-8}$–$10^{-9}$ M. Laser power was varied in the range 0.010–10.0 mW.

**Measurements of Rh6G and FITC in Water.** Figure 6a,b shows AC functions of Rh6G and FITC in water at various laser intensities. At low excitation intensities the slow part of the correlation function was fitted to eq 1; otherwise, in the presence of sample volume distortions, eq 32 was used. These sample volume distortions typically showed up above mean excitation intensities of $10^5$ W/cm$^2$ for Rh6G and $10^4$ W/cm$^2$ for FITC, respectively. The measured values of $\bar{T}_{eq}$ and $\bar{\tau}_T$ were fitted to the expressions of eqs 28 and 29, respectively (Figure 7a,b). At higher excitation intensities, especially for FITC, $\bar{T}_{eq}$ was found to decrease slightly. This probably reflects a higher photodecomposition yield of FITC,[8] which will lead to a stronger concentration depletion in the beam center (see Figure 6). Another effect that might lead to the decrease in $\bar{T}_{eq}$ is the difficulty of aligning the profiles of the CEF$(\bar{r},z)$ and $S_1(\bar{r},z)$ on a maximum fluorescence basis at high intensities due to fluorescence saturation (Figure 4a). Therefore, it is possible that the rate of intersystem crossing of FITC is somewhat underestimated. The fitted parameters of $k_{23}$, $k_{31}$, and $\sigma_{exc}$ are given in Table 1. The fact that $k_{23}$ of FITC was found to be more than five times that of Rh6G is a likely reason for its higher photodecomposition yield. This is also the reason for the lower excitation intensity levels at which sample volume distortions could be observed. The fitted parameters were found to be well reproducible between independent series of measurements. Measurements on Rh6G were repeated with different distributions of detected fluorescence, $\bar{\imath}(\bar{r},z)$, obtained by using a different pinhole size (50 μm) and another microscope objective (40×, 0.9 NA, Zeiss). The obtained parameters of $k_{23}$, $k_{31}$, and $\sigma_{exc}$ were found to be within experimental error of the values determined using the standard setup.

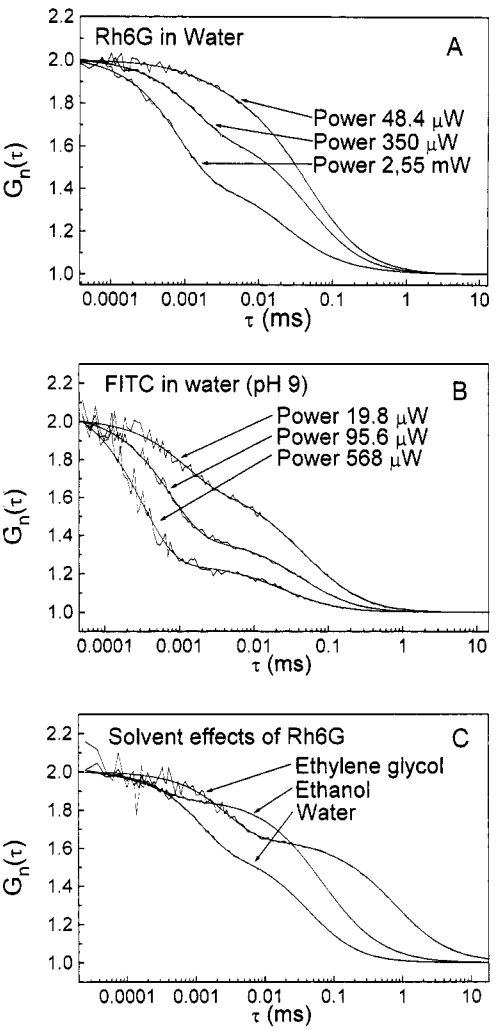


**Figure 6.** FCS curves of Rh6G (A) and FITC (B) measured in water at different excitation intensities (beam radius 0.3 μm, pinhole 30 μm, data acquisition times 100 and 300 s, respectively). Also plotted are the corresponding theoretical curves resulting from fitting the data to eq 34. The amplitudes of the correlation curves have all been normalized to 1. The triplet populations are increased and bunching times are shortened at higher excitation intensities. The effects are more pronounced for FITC. Note the different excitation powers applied and that FITC requires much less excitation intensities to reach a significant triplet population. (C) AC functions of Rh6G in different solvents. Experimental data are plotted for Rh6G in water, ethylene glycol, and ethanol under similar excitation conditions (beam diameter, power, etc.). Data acquisition time was 300 s. The triplet properties are observed to differ considerably.

**Solvent Effects on the Triplet Parameters.** Measurements were also performed on Rh6G in methanol, ethanol, propanol, and ethylene glycol and on FITC in ethanol. The triplet state kinetics of these fluorophores differed substantially between some of these solvents (Figure 6c). The differences are likely to reflect the different polarities, viscosities, and oxygen solubilities of these solvents. In Table 2, the triplet rate parameters for Rh6G in the different solvents are given as well as those of FITC in ethanol.

**Environment Sensing, Quenching Effects.** In the next series of experiments we investigated how well the observed changes in the triplet state rate parameters reflect changes in

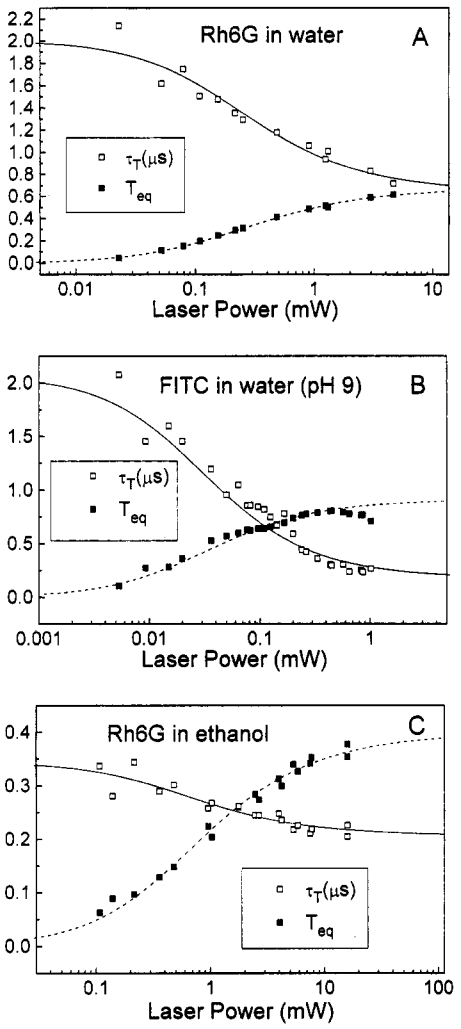


**Figure 7.** The resulting curves of the measured $\bar{\tau}_T$ (open squares) and $\bar{T}_{eq}$ (solid squares) for Rh6G in water (A), FITC in water (B), and Rh6G in ethanol (C) plotted as a function of excitation intensity and the corresponding fittings to eqs 28 and 29.

environmental conditions. Potassium iodide in water was used as a model system, because of its well-known property to quench fluorescence proportionally to its concentration. According to Stern–Volmer theory,

$$k_{12} = \sigma\Phi$$

$$k_{21} = [k_{21}]_0 + K_{Q21}[\mathrm{KI}]$$

$$k_{23} = [k_{23}]_0 + K_{Q23}[\mathrm{KI}]$$

$$k_{31} = [k_{31}]_0 + K_{Q31}[\mathrm{KI}] \qquad (35)$$

where $K_{Q21}$, $K_{Q23}$, and $K_{Q31}$ are the quenching constants of iodide for the $S_1-S_0$, $S_1-T$, and $T-S_0$ transitions, respectively, and [KI] is the concentration of potassium iodide. AC functions were measured at different intensities and at different concentrations of potassium iodide, ranging from 0 to 10 mM. For each concentration, the obtained values of $\bar{\tau}_T$ and $\bar{T}_{eq}$ were plotted as functions of excitation intensity and analyzed as described above. From the time-correlated single-photon-counting measurements, a value of $9.4 \times 10^9$ $M^{-1}$ $s^{-1}$ was obtained for the sum of $K_{Q21}$ and $K_{Q23}$, which was subsequently fixed in the fitting procedure. The effects of iodide could be seen on the AC functions as a strong buildup of the triplet state population as well as a reduced bunching time (Figure 8). The measured

**TABLE 1: Obtained Values of $k_{23}$, $k_{31}$, and $\sigma_{exc}$ for Rh6G and FITC (pH 9) in Water[a]**

| compd | $k_{23}$ (expt) ($\mu s^{-1}$) | $k_{230}$ (ref) ($\mu s^{-1}$) | $k_{31}$ (expt) ($\mu s^{-1}$) | $k_{31}$ (ref) ($\mu s^{-1}$) | $\sigma_{exc}$ (expt) ($10^{-16}$ cm$^2$) | $\sigma_{exc}$ (ref) ($10^{-16}$ cm$^2$) |
|---|---|---|---|---|---|---|
| FITC | 5.7 ± 30% | 6.7[b,18] 12[b,c,7] 11[b,19] 8[b,c,16] 8[b,18] 39[c,d,26] | 0.48 ± 10% | 0.48[b,6] | 3.0 ± 40% | 2.6[56] |
| Rh6G | 1.10 ± 20% | 0.4[c,1] 2.0[17] | 0.49 ± 10% | 0.3[1] | 1.7 ± 20% | 1.8[e,47] |

[a] The accuracy limits are given from the confidence intervals of the fittings to eqs 28 and 29, respectively, with an added error assuming an inaccuracy of 10–20% in the measured excitation intensity. For comparison, data from literature is included. [b] Fluorescein. [c] Deoxygenated. [d] pH 7. [e] At 528 nm excitation.

**TABLE 2: Obtained Values of Intersystem Crossing, $k_{23}$, and Triplet Decay Rate, $k_{31}$, of Rh6G and FITC in Some Different Solvents[a]**

| compd | solvent | $k_{23}$ (expt) ($\mu s^{-1}$) | $k_{23}$ (ref) ($\mu s^{-1}$) | $k_{31}$ (expt) ($\mu s^{-1}$) | $k_{31}$ (ref) ($\mu s^{-1}$) |
|---|---|---|---|---|---|
| Rh6G | water | 1.10 ± 20% | see Table 1 | 0.49 ± 10% | see Table 1 |
| | methanol | 3.0 ± 20% | 20[23] 0.61[e,13] | 3.5 ± 10% | 7.1[23] 0.51[e,13] |
| | ethanol | 2.0 ± 20% | 0.42[12] 1.8[b,21] 0.53[13] 3.4[22] 28[64] 2.1[66] | 2.9 ± 10% | 2.2[12] 4.0[21] 0.25[13] 4.0[22] 11[64] 3.0[66] |
| | propanol | 2.5 ± 20% | 0.75[11] | 2.5 ± 10% | 1.2[11] |
| | ethylene glycol | 0.35 ± 30% | 0.64[27] 6.4[67] 0.38[13] | 0.20 ± 10% | 0.25[27] 8.0[67] 0.13[13] |
| FITC | water (pH 9) | 5.7 ± 30% | see Table 1 | 0.48 ± 10% | see Table 1 |
| | ethanol | 9.0 ± 30% | 7.6[c,18] 8.75[c,d,16] | 2.9 ± 10% | no ref found |

[a] There is in many cases a big diversity in the data reported in the literature. [b] Should be multiplied by $\sigma_{tn}/\sigma_{21}$, where $\sigma_{tn}$ = absorbtion cross section of the triplet state and $\sigma_{21}$ = stimulated emission cross section. [c] Fluorescein. [d] Deoxygenated. [e] Deuterated.

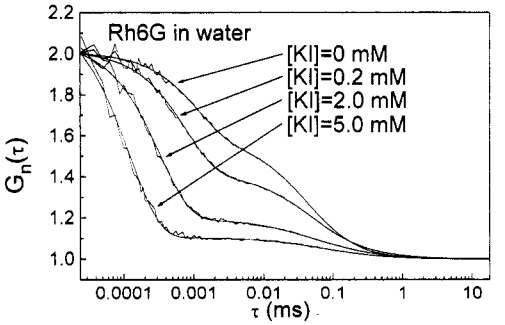


**Figure 8.** FCS curves of Rh6G in water at different concentrations of potassium iodide. (Excitation power 0.10 mW, beam radius 0.3 $\mu$m, pinhole diameter 30 $\mu$m, data acquisition time 100 s. The amplitudes of the correlation curves have all been normalized to 1.)

values of $k_{31}$ and $k_{23}$ display a linear dependence on the iodide concentration (Figure 9b,c). The lack of data for the quenching of Rh6G by iodide in aqueous solution in combination with a high variability of reported values between different fluorophores, solutions, pH, and temperatures[14] makes a comparison difficult. The obtained values of $K_{Q23}$ and $K_{Q31}$ are comparable to what has been reported for similar systems (quenching of anthracene by KI in water/EtOH 1:1 $K_{Q23} = (3.9 \pm 0.3) \times 10^9$

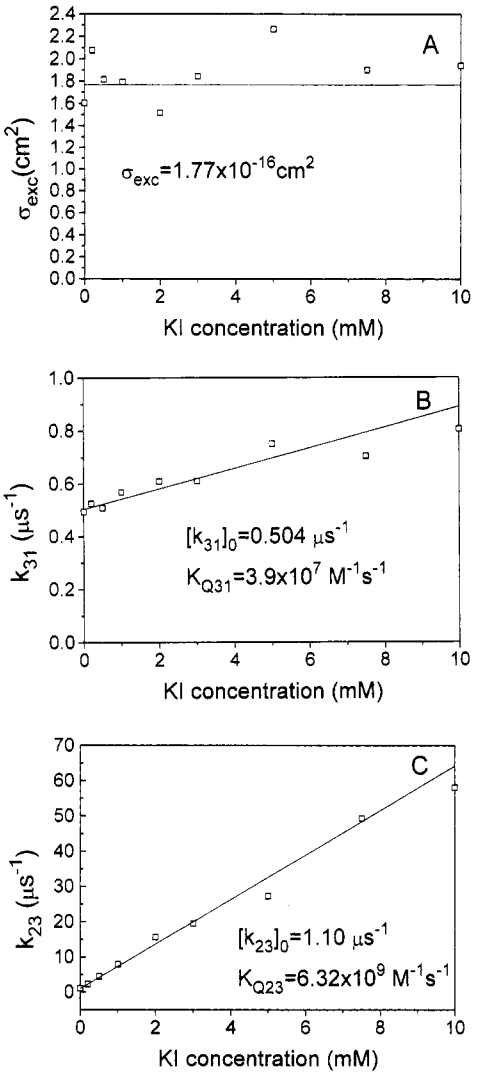


**Figure 9.** Excitation cross section, $\sigma_{exc}$ (A), decay rate of the triplet state, $k_{31}$ (B), and rate of intersystem crossing, $k_{23}$, of Rh6G (C), as a function of potassium iodide (KI) concentration. The obtained values were fitted to linear equations with the fitted parameters shown in each of the diagrams, respectively.

$M^{-1}$ $s^{-1}$ [57,58] and of EITC in water $K_{Q31} = 1.5 \times 10^7$ $M^{-1}$ $s^{-1}$ [59]). At concentrations of potassium iodide exceeding 5 mM the strong enhancement of $k_{23}$ may make the assumption of eq 11 obsolete. The algorithms for obtaining $\bar{\tau}_T$ and $\bar{T}_{eq}$ should therefore be used with some caution. This might be the reason for the slight deviation from linearity seen for $k_{23}$ and $k_{31}$ at the highest iodide concentrations (Figure 9) and could also lead to an underestimation of $K_{Q23}$ and $K_{Q31}$. However in general, this does not set a limitation to the analysis. When investigating fluorophores having high rates of intersystem crossing, one could, in principle, use the full expressions for the eigenvalues and eigenvectors of eq 10 or use some appropriate numerical method[60] to calculate them.

In addition to potassium iodide, the quenching by oxygen was studied. Oxygen is known to be a potent quencher of the triplet state of Rh6G.[1,12,13,21,22,27] Although, in principle, having the same impact on the rate parameters as iodide, the presence of oxygen is believed to have an opposite effect on the triplet population due to a higher $K_{Q31}$ than $K_{Q23}$.[23,61] Consequently for Rh6G equilibrated with a pure oxygen atmosphere, the triplet population should decrease considerably. We observed this phenomenon (Figure 10) and found the triplet decay rate increased by a factor of 5 to a value $2.5 \times 10^6$ $s^{-1}$, while the rate of intersystem crossing was only approximately doubled.

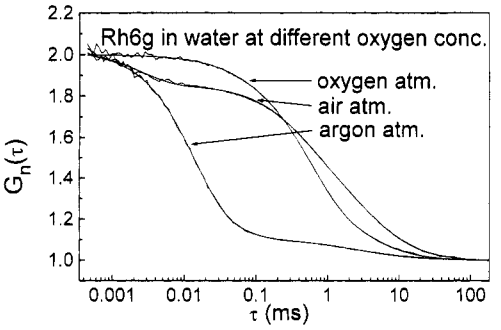


**Figure 10.** Sample of three correlation curves for droplets of Rh6G solution measured in argon, air, and oxygen atmospheres, respectively, and their corresponding fitted curves according to eq 34. The fitting of the curves measured in oxygen atmosphere revealed a considerable exponential term, most likely being generated by photodegradation. (Excitation power 6.25 mW, beam radius 2.5 μm, pinhole radius 125 μm, data acquisition time 300 s. The amplitudes of the correlation curves have all been normalized to 1.)

In the deoxygenated case, the determination of $k_{31}$ was complicated by the fact that the lifetime of the triplet state of Rh6G far exceeded the time of diffusion in and out of the sample volume element. Therefore, the fluorescence fluctuations due to singlet−triplet interactions could no longer be treated as independent of those due to translational diffusion. For this reason the sample volume element was increased by reducing the focusing of the laser beam ($\omega_1$ being 2.5 μm) and by using a bigger pinhole radius (125 μm). The strongly extended bunching time at low intensities might have induced some inaccuracy in the determinations of $k_{31}$. Other deactivation processes of the triplet state, such as delayed fluorescence and energy circulation effects, might be of some importance in the absence of oxygen quenching. The value of $k_{31}$ in argon atmosphere was found to be on the order 2.5 $ms^{-1}$, and $k_{23}$ was decreased to about $0.6 \times 10^6$ $s^{-1}$. The value of $k_{23}$ was calculated from a series of $\lambda_3$ values measured at different intensities with the normal beam radius (0.3 μm) and pinhole (radius 15 μm). The two rate constants, $k_{23}$ and $k_{31}$, can be seen to be approximately linearly dependent on oxygen concentration. Assuming oxygen concentrations of 0, 0.28, and 1.4 mM in argon, air, and oxygen atmospheres, respectively,[6] $K_{Q23}$ and $K_{Q31}$ could be estimated to be $(1.0 \pm 0.3) \times 10^9$ and $(1.8 \pm 0.2) \times 10^9$ $M^{-1}$ $s^{-1}$, respectively. The value of $K_{Q31}$ is somewhat higher than what has been reported in earlier investigations ($9 \times 10^8$ and $(0.25-1.64) \times 10^9$ $M^{-1}$ $s^{-1}$ for $K_{Q31}$ of oxygen in water and ethanol, respectively[1,12,24]). The presence of oxygen strongly reduces the population of the triplet state. On the other hand, in oxygen atmosphere the FCS curve can be seen to decay faster than that measured in air (Figure 10). This is most likely caused by a higher photodecomposition yield. One can conclude that for the effects of oxygen on fluorescence there is a trade-off between a reduced triplet population and a higher photodecomposition rate. This is in agreement with what has been shown previously in the case of Rh6G dye lasers.[23] For the experimental conditions presented here, the optimum oxygen concentration for Rh6G was found to be close to that in air (0.2 atm oxygen).

## Concluding Remarks

**General Methodological Aspects.** To make a more accurate determination of the excitation cross section, $\sigma_{exc}$, and of $k_{23}$, it seems necessary to calculate $\bar{\tau}_T$ and $\bar{T}_{eq}$ three-dimensionally over the sample volume element. In our previous report[30] $\bar{\lambda}_3$ and $\bar{T}_{eq}$ were calculated from the simplified assumption that the power of the laser was evenly distributed over the sample

volume element as $I = P/\pi\omega_1^2$. When comparing the analysis used previously to that given here using the same set of experimental data, one can conclude that while the estimation of $k_{31}$ is essentially the same, $k_{23}$ is with the simplified analysis 15−40% less. The higher deviations are found in the case of a wider range of CEF and a large ratio of $k_{23}$ to $k_{31}$. The differences are due to the changes of the sample volume element ($\bar{i}(\bar{r},z)$) that will occur at different excitation intensities. These changes are not accounted for in the previous analysis. However, when measuring with a small pinhole on a fluorophore having a moderate $k_{23}/k_{31}$, this analysis can provide a good approximation with a much reduced analysis effort. For the determination of diffusion coefficients and concentrations from FCS data, the intensity dependent changes of the sample volume element must also be taken into consideration. These changes are determined by the triplet and saturation properties of the fluorophore under investigation and can differ considerably between different fluorophores, excitation intensities, solvents, and other environmental parameters. The analysis presented in this work relies upon a proper determination of the laser beam characteristics and the distribution of the detected fluorescence intensity, $\bar{i}(\bar{r},z)$. To improve the accuracy, one could consider measuring the laser beam dimensions more carefully, for instance as proposed by Schneider and Webb,[62] and including effects of bleaching. Spherical aberrations and other effects that would lead to a deviation of the image and beam shape have not been considered in this work. As was pointed out,[39] the measured values of $\omega_2/\omega_1$ are considerably larger than those calculated from eq 5. This is believed to be due to spherical aberration. However, assuming the distortion due to spherical aberration to affect both the laser beam and the image equally, the calculated values of $k_{23}$ and $k_{31}$ will not be affected. It is also necessary to confirm for each fluorophore under investigation that additional photophysical reaction pathways can be excluded or otherwise included in the three-state electron model used here. The effects of photobleaching should be the object of further investigation. The FCS measurements have all been performed on small and relatively fast diffusing molecules. If one studies more slowly moving units, like proteins or receptors on a cell surface, the diffusion times through the sample volume element will be long enough to make the effects of photobleaching much more pronounced. Sample volume distortions arise due to saturation and are proportional to the extent of triplet state buildup. The extent of photobleaching is likewise believed to be proportional to the triplet state population. Consequently, it is of importance, if FCS measurements are made at high excitation intensities, to know the triplet properties of the fluorophore, not only to be able to reach optimum fluorescence conditions but also to be able to ascertain when such distortions as those described above will occur and to allow for the appropriate corrections.

**Prospects for the Future.** Considering the variability of the reported values of the triplet state parameters, triplet state monitoring by FCS is likely to produce a more accurate determination. Of special interest are fluorophores that like Rh6G have moderate triplet quantum yields. For those fluorophores, difficulties in the determination of the triplet parameters have been more pronounced in earlier investigations. With very few exceptions, previous measurements of transients in the microsecond time domain have been determined with the use of pulsed excitation and a separate probing beam. A method that comes close to ours is that proposed by Thiel and Drexhage.[27] It requires two CW lasers and the additional knowledge of the flow speed in the dye jet where the fluorophores are investigated. In our method, only a single CW laser is required and the instrumentation is in general much less complicated than, for instance, that used in flash photolysis. Neither knowledge of the absorption cross section of the triplet state nor that of the absolute concentration is necessary. Another advantage of FCS is the high sensitivity which allows triplet measurements to be performed on a very low number of molecules. The data presented on potassium iodide quenching suggest that FCS could be used as an alternative method to traditional steady state fluorescence quenching measurements. The relatively high environmental sensitivity of the triplet rate parameters in combination with the sensitivity of FCS should be considered as a means of investigating other environmental parameters as well. One should consider the idea of investigating how triplet state parameters of pH-, voltage-, and calcium-sensitive dyes behave due to environment. It could be of interest to relate the results shown in Figure 10 to the detection performance of optical sensors used to monitor oxygen concentration. Most of them are based on the measurement of the decrease in fluorescence intensity.[63] Quenching of phosphorescence offers a much higher relative change due to the longer lifetime, but the sensitivity will not be as good. Combining the sensitivity of fluorescence with the longer lifetimes of phosphorescence, it should be possible to measure accurately low oxygen concentrations in small local environments. The excitation intensity can be adapted so that the relative change in $\bar{T}_{eq}$ or $\bar{\tau}_T$ will be proportional to the relative change in oxygen concentration. This will give the measurement technique a very high dynamic range. Another potential application is the use of FCS together with an analysis similar to that presented here to study fluorescence energy transfer. The obvious advantage using FCS would be the extended time scale over which such energy transfer processes could be seen combined with an outstanding sensitivity. In general, the fluctuations generated by singlet−triplet transitions will, since they are independent of those due to translational diffusion, provide an additional set of measurable parameters which will increase the information obtainable in FCS measurements.

**Acknowledgment.** We thank Prof. Måns Ehrenberg, BMC Uppsala University, for valuable discussions and Dr. Kurt Berndt, Dr. Johannes Dapprich, and Dr. Torleif Härd for comments on the manuscript. This work was supported by the Swedish National Science Research Council and the Swedish Research Council for Engineering Sciences as well as by funds from the Karolinska Institute.

## References and Notes

(1) Korobov, V. E.; Chibisov, A. K. *J. Photochem.* **1978**, *9*, 411.
(2) Lüttke, W.; Schäfer, F. P. *Laser und Optoelektronik* **1983**, *2*, 127.
(3) Weber, J. *Opt. Comm.* **1973**, *7*, 420.
(4) Rylkov, V. V.; Cheshev, E. A. *Opt. Spectrosc. (USSR)* **1987**, *63*, 608.
(5) Mathies, R. A.; Peck, K.; Stryer, L. *Anal. Chem.* **1990**, *62*, 1786.
(6) Kasche, V.; Lindqvist, L. *J. Phys.Chem.* **1964**, *68*, 817.
(7) Bowers, P. G.; Porter, F. R. S. *Proc. R. Soc. London Ser. B* **1967**, *299*, 348.
(8) Lindqvist, L. *Ark. Kemi* **1960**, *16*, 79.
(9) Beaumont, P. C.; Johnson, D. G.; Parsons, B. J. *J. Chem. Soc. Faraday Trans.* **1993**, *89*, 4185.
(10) Penzkofer, A.; Beidon, A. *Chem. Phys.* **1993**, *177*, 203.
(11) Korobov, V. E.; Shubin, V. V.; Chibisov, A. K. *Chem. Phys. Lett.* **1976**, *45*, 498.
(12) Dempster, D. N.; Morrow, T.; Quinn, M. F. *J. Photochem.* **1973**, *2*, 343.
(13) Asimov, M. M.; Gavrilenko, V. N.; Rubinov, A. N. *J. Lumin.* **1990**, *46*, 243.
(14) Korobov, V. E.; Chibisov, A. K. *Russ. Chem. Rev.* **1983**, *52*, 27.
(15) Korobov, V. E.; Chibisov, A. K. *Opt. Spectrosc. (USSR)* **1975**, *38*, 706.

(16) Soep, B.; Kellman, A.; Martin, M.; Lindqvist, L. *Chem. Phys. Lett.* **1972**, *13*, 241.
(17) Ketsle, G. A.; Levshin, L. V.; Bryukhanov, V. V. *J. Appl. Spectrosc. (USSR)* **1975**, *24*, 809.
(18) Gandin, E.; Lion, Y.; Van de Vorst, A. *Photochem. Photobiol.* **1983**, *37*, 271.
(19) Usui, Y. *Chem. Lett.* **1973**, 743.
(20) Petsold, O. M.; Byteva, I. M.; Gurinovich, G. P. *Opt. Spectrosc. (USSR)* **1973**, *34*, 599.
(21) Strome, F. C., Jr. *IEEE J. Quantum Electron* **1972**, *8*, 98.
(22) Webb, J. P.; McColgin, W. C.; Peterson, O. G.; Stockman, D. L.; Eberley, J. H. *J. Chem. Phys.* **1970**, *53*, 4227.
(23) Schäfer, F. P.; Ringwelski, L. *Z. Naturforsch.* **1973**, *28a*, 792.
(24) Smolskaya, T. S.; Rubinov, A. N.; Asimov, M. M. *Opt. Spectrosc. (USSR)* **1973**, *34*, 410.
(25) Dzhasim, S. Y.; Serov, N. Y.; Fadeev, V. V.; Chekalyuk, A. M. *J. Appl. Spectrosc. (USSR)* **1992**, *56*, 252.
(26) Viappiani, C. *Biophys. Chem.* **1994**, *50*, 293.
(27) Thiel, E.; Drexhage, K. H. *Chem. Phys. Lett.* **1992**, *199*, 329.
(28) Pavlopoulos, T. G.; Golich, D. J. *J. Appl. Phys.* **1988**, *64*, 521.
(29) Bernard, J.; Fleury, L.; Talon, H.; Orrit, M. *J. Chem. Phys.* **1993**, *98*, 850.
(30) Widengren, J.; Rigler, R.; Mets, U. *J. Fluoresc.* **1994**,4, 255.
(31) Elson, E. L.; Magde, D. *Biopolymers* **1974**, *13*, 1.
(32) Koppel, D. E. *Phys. Rev. A* **1974**, *A10*, 1938.
(33) Ehrenberg, M.; Rigler, R. *Chem. Phys.* **1974**, *4*, 390.
(34) (a) Magde, D.; Elson, E. L.; Webb, W. W. *Biopolymers* **1974**, *13*, 29. (b) Magde, D.; Webb, W. W.; Elson, E. L. *Biopolymers* **1978**, *17*, 361.
(35) Aragon, S. R.; Pecora, R. *J. Chem. Phys.* **1976**, *64*, 1791.
(36) Kask, P.; Piksarv, P.; Mets, U.; Pooga, M.; Lippmaa, E. *Eur. Biophys. J.* **1987**, *14*, 257.
(37) Rigler, R.; Widengren, J.; Mets, U. In *Fluorescence Spectroscopy*; Wolfbeis, O. S., Ed.; Springer Verlag: Berlin, 1992; pp 13−24.
(38) (a) Rigler, R.; Mets, U. *SPIE* **1992**, *1921*, 239. (b) Mets, U.; Rigler, R. *J. Fluoresc.* **1994**, *4*, 259.
(39) Rigler, R.; Mets, U.; Widengren, J.; Kask, P. *Eur. Biophys. J.* **1993**, *22*, 169.
(40) Rigler, R.; Widengren, J. *Bioscience*; Lund University Press: Lund, 1990; 180−183
(41) Marquardt, D. W. *J. Soc. Ind. Appl. Math.* **1963**, *11*, 431.
(42) Rigler, R.; Claesens, F.; Lomakka, G. In *Ultrafast Phenomena IV*; Auston, D. H., Eisenthal, K. B., Eds.; Springer-Verlag: Berlin−Heidelberg, 1984; pp 467−472.
(43) Qian, H.; Elson, E. L. *Appl. Opt.* **1991**, *30*, 1185.
(44) Moerner, W. E.; Basche', T. *Angew. Chem., Int. Ed. Engl.* **1993**, *32*, 457.
(45) Orrit, M.; Bernard, J.; Personov, R. I. *J. Phys. Chem.* **1993**, *97*, 10256.
(46) de Vries, H.; Wiersma, D. A. *J. Chem. Phys.* **1979**, *70*, 5807.
(47) Penzkofer, A.; Falkenstein, W.; Kaiser, W. *Chem. Phys. Lett.* **1976**, *44*, 82.
(48) Rylkov, V. V.; Chesev, E. A. *Opt. Spectrosc. (USSR)* **1987**, *63*, 462.
(49) Penzkofer, A.; Leupacher, W. *J. Lumin.* **1987**, *37*, 61.
(50) Soper, S. A.; Davis, L. M.; Fairfield, F. R.; Hammond, M. L.; Harger, C. A.; Jett, J. H.; Keller, R. A.; Marrone, B. L.; Martin, J. C.; Nutter, H. L.; Shera, E. B.; Simpson, D. J. *SPIE* **1991**, *1435*, 168.
(51) Basche', T.; Moerner, W. E.; Orrit, M.; Talon, H. *Phys. Rev. Lett.* **1992**, *69*, 1516.
(52) Kask, P.; Piksarv, P.; Mets, U. *Eur. Biophys. J.* **1985**, *12*, 163.
(53) Saleh, B. *Photoelectron Statistics*; Springer Verlag: Berlin, Heidelberg, 1978; p 72.
(54) Crank, J. *The Mathematics of Diffusion*; Clarendon Press: Oxford, 1975.
(55) Peters, R.; Brünger, A.; Schulten, K. *Proc. Natl. Acad. Sci. U.S.A* **1981**, *78*, 962.
(56) Haugland, R. P. *Handbook of Fluorescent Probes and Research Chemicals*; Molecular Probes: Eugene, OR, 1992; p 218.
(57) Shizuka, H.; Nakamura, M.; Morita, T. *J. Chem. Phys.* **1980**, *84*, 989.
(58) Mac, M.; Najbar, J.; Phillips, D.; Smith, T. A. *J. Chem. Soc., Faraday Trans.* **1992**, *88*, 3001.
(59) Corin, A. F.; Blatt, E.; Jovin, T. M. *Biochemistry* **1987**, *26*, 2207.
(60) Press, W. H.; Flannery, B. P.; Teukolsky, S. A.; Vetterling, W. T. *Numerical Recipes*; Cambridge University Press: Cambridge, 1986; p 335.
(61) Marling, J. B.; Gregg, D. W.; Thomas, S. J. *IEEE J. Quantum Electron.* **1979**, *6* (9), 570.
(62) Schneider, M. B.; Webb, W. W. *Appl. Opt.* **1981**, *20*, 1382.
(63) Liu, Y. M.; Pereiro-Garcia, R.; Valencia-Gonzalez, M. J.; Diaz-Garcia, M. E.; Sanz-Medel, A. *Anal. Chem.* **1994**, *66*, 836.
(64) Snavely, B. B. *Proc. IEEE* **1969**, *57*, 1374.
(65) Self, S. A. *Appl. Opt.* **1983**, *22*, 658.
(66) Aristov, A. V.; Maslyukov, Y. S. *Opt. Spectrosc. (USSR)* **1973**, *35*, 1138.
(67) Teschke, B.; Dienes, A.; Holtom, G. *Opt. Commun.* **1975**, *13*, 318.

JP950780B